

PAPER

# Absence of magnetic ordering in the spin liquid candidate $\text{Ca}_3\text{Cu}_2\text{GeV}_2\text{O}_{12}$

To cite this article: Joey A Lussier *et al* 2020 *J. Phys.: Condens. Matter* **32** 134001

View the [article online](#) for updates and enhancements.



**IOP | ebooks™**

Bringing you innovative digital publishing with leading voices  
to create your essential collection of books in STEM research.

Start exploring the collection - download the first chapter of  
every title for free.

# Absence of magnetic ordering in the spin liquid candidate $\text{Ca}_3\text{Cu}_2\text{GeV}_2\text{O}_{12}$

Joey A Lussier<sup>1</sup>, Brooke N Richtik<sup>1</sup>, Cole Mauws<sup>2</sup>, Jeffrey W Lynn<sup>4</sup>  
and Chris R Wiebe<sup>1,2,3</sup>

<sup>1</sup> Department of Chemistry, University of Winnipeg, Winnipeg, Canada

<sup>2</sup> Department of Chemistry, University of Manitoba, Winnipeg, Canada

<sup>3</sup> Canadian Institute for Advanced Research, Toronto, Ontario, Canada

<sup>4</sup> NIST Center for Neutron Research, National Institute of Standards and Technology, Gaithersburg, MD, United States of America

E-mail: [joeylussier@gmail.com](mailto:joeylussier@gmail.com)

Received 29 August 2019, revised 13 November 2019

Accepted for publication 27 November 2019

Published 27 December 2019



## Abstract

Typically, quantum spin liquid candidates can be found in materials with a combination of geometrical frustration along with low spin. Due to its spin of  $S = 1/2$  the copper (II) ion is often present in the discussion on spin liquid candidates. The solid state compound  $\text{Ca}_3\text{Cu}_2\text{GeV}_2\text{O}_{12}$  is a material that crystallizes in the garnet structure (s.g. #230,  $Ia-3d$ ), where 3D frustration is known to occur. Heat capacity has shown a lack of magnetic ordering down to 0.35 K, confirmed with low temperature neutron diffraction to 0.07 K. This system displays a Weiss temperature of  $-0.93(1)$  K indicating net antiferromagnetic interactions and significant  $J_1$ - $J_2$  competition causing frustration. Using both neutron and x-ray diffraction along with heat capacity and magnetometry, the work presented here shows  $\text{Ca}_3\text{Cu}_2\text{GeV}_2\text{O}_{12}$  has potential as a new spin liquid candidate.

Keywords: quantum spin liquid, frustrated magnetism, garnet, quantum materials

(Some figures may appear in colour only in the online journal)

## 1. Background and introduction

Interest in the field of frustrated magnetism in solid state materials has been steadily increasing over the last decade due to the vast amount of unusual ground states that they exhibit [1, 2]<sup>5,6</sup>. Frustration is often found when competing interactions prevent traditional magnetic ordering of the local spin configurations [3]. One of the simplest examples of frustration in two dimensions occurs when competing antiferromagnetic interactions exist between spins on the 2D square lattice. This ' $J_1$ - $J_2$ ' model, where  $J_1$  and  $J_2$  denote the nearest neighbour  $J_1$  and next nearest neighbour interactions  $J_2$ , respectively, leads to spin liquid behaviour at low temperatures [4, 5]. A quantum spin liquid is a largely elusive state of matter with quantum disordered ground states preventing conventional magnetic ordering [6, 7]. Depending on the context, a variety of

definitions have been used for quantum spin liquids, including: the absence of long range order; the absence of spontaneously broken symmetry; or a state with fractional excitations [8]. Typically, many different observations from different techniques are required to build a complete picture of a true spin liquid [6]. Small spins (ie.  $S = 1/2$ ) which enhance quantum fluctuations are often included in the criteria for new quantum spin liquids [1, 9, 10]<sup>7</sup>. The  $J_1$ - $J_2$  model on the square lattice in two dimensions is a clear example of a quantum spin liquid, although it is difficult to realize true 2D  $S = 1/2$  systems in bulk 3D materials. Other examples of quantum spin liquid candidates in 2D systems are usually found in lattices based upon triangular topologies such as the kagomé system Herbertsmithite [11] and the triangular lattice  $\text{TbInO}_3$  [12].

In three dimensions, the case is less clear for spin liquid behaviour and for spin liquid candidates. Much of the search for new spin liquids has concentrated on triangular plaquette

<sup>5</sup> For a review, see [1].

<sup>6</sup> For a review of quantum spin liquids in frustrated materials, see [2].

<sup>7</sup> See footnote 5.

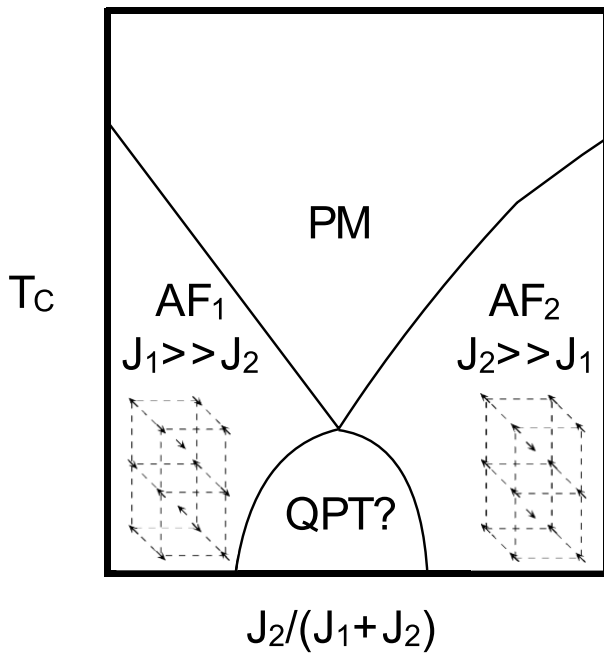


**Figure 1.** Generic phase diagram of the  $S = 1/2$  bcc lattice with nearest ( $J_1$ ) and next nearest neighbour ( $J_2$ ) interactions. The paramagnetic (PM) region, ordered ( $AF_1$ ,  $AF_2$ ) region and a quantum phase transition (QPT) at  $J_1/J_2 = 0.705 \pm 0.005$  are noted. Adapted from [15].

systems connected in various ways, such as the pyrochlore lattice (made of 3D corner-shared tetrahedra) [13] and the face centred cubic (FCC) lattice (made of 3D edge-shared tetrahedra) [14]. However, for spins connected through the body centred cubic (BCC) lattice in three dimensions, there has been considerably less attention, even though frustration clearly is present if there is competing  $J_1$ – $J_2$  superexchange with nearest and next nearest neighbour spins. In the quantum case for  $S = 1/2$  in particular, a significant amount of theory has been developed to explore how quantum fluctuations modify the classical phase diagram separating two antiferromagnetically ordered phases for dominant  $J_1$  or  $J_2$  interactions. Oitmaa and Zheng, for example, have reported that competition between nearest neighbour  $J_1$  and next nearest neighbour  $J_2$  on the BCC lattice leads to a phase diagram with a paramagnetic critical line separating the two ordered antiferromagnetic phases at  $J_1/J_2 = 0.705 \pm 0.005$  for the case of  $S = 1/2$  spins (figure 1) [15]. Series expansion calculations have shown that this is a first-order transition for finite temperature, but the phase boundary extending down to zero Kelvin ends in a quantum phase transition. Quantum fluctuations can allow for a new phase to exist near this critical  $J_1/J_2$  value and shift the boundaries of this phase diagram considerably. Very recent theoretical work has shown that the phase diagram for this system can be even more complex for nearest neighbour  $J_1$ , next nearest neighbour  $J_2$  and third neighbour  $J_3$  interactions on the BCC lattice. The full quantum phase diagram allows for six different phases, including traditional Néel ordering, a ferromagnetic ordered phase, a stripe ordering, and a quantum paramagnetic state [16]. These findings strongly motivate a search for model  $S = 1/2$  systems on the BCC lattice that can be tuned to have varying  $J_1/J_2/J_3$  interactions to explore the effects of frustration.

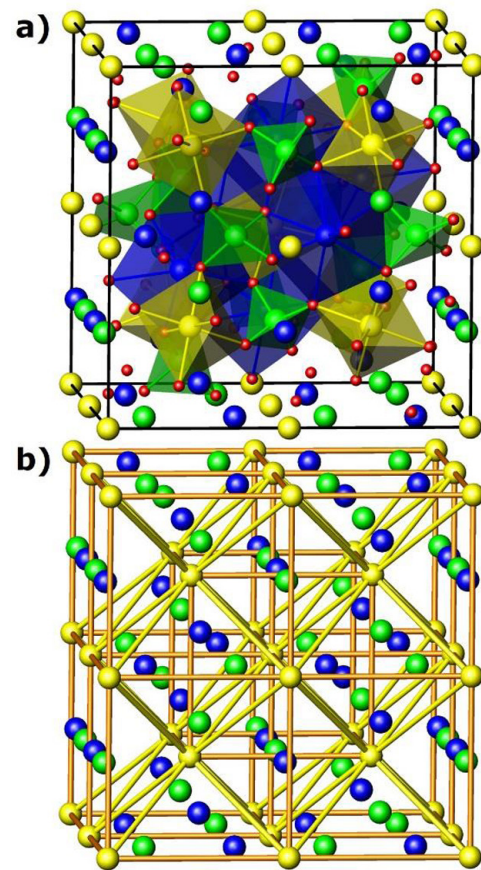


**Figure 2.** Illustrations of the garnet structure highlighting polyhedra (a) and Cu–Cu bonds (b). Blue =  $Ca^{2+}$ ; yellow =  $Cu^{2+}$ ; green = Ge/V mixed cations. Nearest neighbour bonds are shown in yellow; second-nearest neighbour bonds are shown in orange.

Transition metals in particular have large, extended d orbitals which can give rise to significant overlap with nearest neighbours, and likely provide some of the best examples of significant superexchange on the BCC lattice.

The garnets are a well studied family of materials isostructural with the mineral garnet, with the general formula  $A_3B_2C_3X_{12}$ . Figure 2(a) shows the garnet structure where A (blue), B (yellow), and C (green) refer to cations in dodecahedral, octahedral, and tetrahedral sites, respectively. X (red) is typically the oxide anion; however fluoride and hydroxide garnets are also known [17]. Most garnets crystallize in the cubic  $Ia\bar{3}d$  space group (s.g. #230) with 8 formula units per unit cell. The A cation is found in the 24c site ( $1/8, 0, 1/4$ ), the B cation is found in the 16a site (0, 0, 0), the C-cation in the 24d site ( $3/8, 0, 1/4$ ), and the X anion in the 96h general position ( $x, y, z$ ). Most importantly for this work, the B cation is found in a body-centred cubic (bcc) sublattice. Figure 2(b) shows this bcc sublattice, where the nearest neighbours are indicated with yellow bonds and the second-nearest neighbours are shown connected with an orange bond (which can be directly linked to the predictions of Oitmaa and Zheng's exchange pathways [15]). Due to their structural tolerance, many cations can be substituted into a garnet [17], and if the proper choice of cations in the A and C positions are realized, the  $Cu^{2+}$  cation can be found in a bcc lattice. Examples of this include  $NaCa_2Cu_2V_3O_{12}$

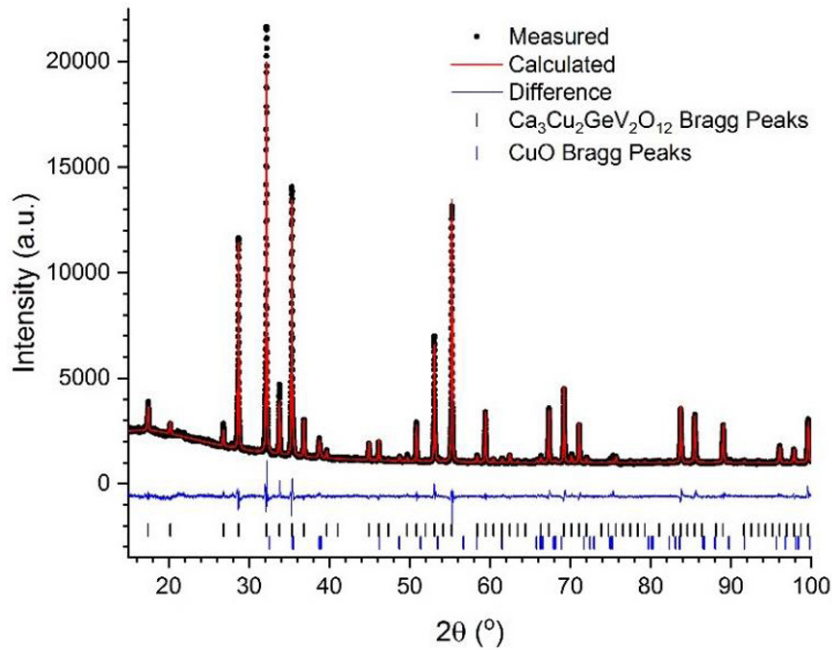


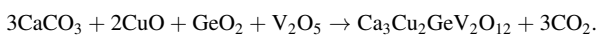
**Figure 3.** Rietveld plot of the powder x-ray diffraction data for the refinement of the cubic garnet phase  $\text{Ca}_3\text{Cu}_2\text{GeV}_2\text{O}_{12}$  with a small CuO impurity. Black symbols = observed data, red line = fit, blue line = difference. Bragg peak positions are shown as black ticks for the garnet phase and blue ticks for the CuO phase.

[18],  $\text{Mn}_3\text{Cu}_2\text{SiV}_2\text{O}_{12}$  [19],  $\text{SrCaNaCu}_2\text{V}_3\text{O}_{12}$  [20], and  $\text{Ca}_3\text{Cu}_2\text{GeV}_2\text{O}_{12}$  [21]. In this article we will focus on the  $S = 1/2$   $\text{Ca}_3\text{Cu}_2\text{GeV}_2\text{O}_{12}$  garnet reported by Mill *et al* [21]. This compound was synthesized using the conventional solid state method with a small amount of impurity. The structure was refined using the Rietveld method in the original work [22], but to our knowledge no magnetic studies have been performed on this compound. Therefore, the primary motivation behind this work is to understand the magnetic properties of the spin- $1/2$   $\text{Cu}^{2+}$  on the bcc lattice of the spin liquid candidate  $\text{Ca}_3\text{Cu}_2\text{GeV}_2\text{O}_{12}$ .

## 2. Experimental details

### 2.1. Synthesis

Bulk polycrystalline samples were synthesized using the conventional solid-state method.  $\text{CaCO}_3$  (Alfa Aesar, 99.5%),  $\text{CuO}$  (Baker Analyzed Reagent, 99%),  $\text{GeO}_2$  (Alfa Aesar, 99.99%), and  $\text{V}_2\text{O}_5$  (Alfa Aesar, 99.6%) were ground using an agate mortar and pestle in an acetone slurry according to the following scheme:



Reagents were pressed into pellets, placed in an alumina crucible and heated in air for 36h with intermittent grindings every 12h.

### 2.2. Powder x-ray diffraction

Powder x-ray diffraction data were collected on a Huber G670 Guinier Camera diffractometer using  $\text{Cu K}\alpha_1$  radiation (Ge-monochromator,  $\lambda(\text{Cu-K}\alpha_1) = 1.540560 \text{ \AA}$ ). Samples

**Table 1.** Structural parameters for  $\text{Ca}_3\text{Cu}_2\text{GeV}_2\text{O}_{12}$  garnet phase (space group:  $Ia\bar{3}d$  (#230)) as obtained from Rietveld Refinement against x-ray diffraction data measured at room temperature.

Composition		$\text{Ca}_3\text{Cu}_2\text{GeV}_2\text{O}_{12}$
Space group		$Ia\bar{3}d$ (#230)
Unit cell	$a$ ( $\text{\AA}$ )	12.434 08 (9)
	$V$ ( $\text{\AA}^3$ )	1922.39 (4)
$\text{Ca}$ (24c) ( $1/8, 0, 1/4$ )	$B_{\text{iso}}$ ( $\text{\AA}^2$ )	0.73 (3)
$\text{Cu}$ (16a) (0, 0, 0)	$B_{\text{iso}}$ ( $\text{\AA}^2$ )	0.86 (2)
$\text{Ge/V}$ (24d) ( $3/8, 0, 1/4$ )	Occupancy	33%/66%
	$B_{\text{iso}}$ ( $\text{\AA}^2$ )	0.24 (2)
$\text{O}$ (96h) ( $x, y, z$ ) <sup>a</sup>	$x/a$	-0.0369
	$y/b$	0.0550
	$z/c$	0.1556
	$B_{\text{iso}}$ ( $\text{\AA}^2$ )	1.25 (4)
$Z$		8
$R$ -values:		XRD <sup>b</sup> : (Rp, Rwp, $\chi^2$ ) 2.92/4.18/1.60

<sup>a</sup> Oxygen anion positions  $x$ ,  $y$ , and  $z$  were not refined in this work, they were fixed to the positions reported by Mill *et al* [21].

<sup>b</sup> X-ray:  $\text{K}\alpha_1$ ,  $\lambda = 1.540598 \text{ \AA}$ ,  $15^\circ \leq 2\theta \leq 100^\circ$ ,  $\Delta 2\theta = 0.005^\circ$ , 17000 data points.

were mounted as thin layers on a Mylar polyester film using acetone slurries. Data were collected in  $0.005^\circ$  steps covering a  $2\theta$  range from  $15^\circ$  to  $100^\circ$  with 5 min exposure time. Rietveld Refinements were performed using Topas (Version 6) software.

### 2.3. Magnetic properties

DC magnetometry data were collected using a Quantum Design Physical Property Measurement System (PPMS) with a vibrating sample magnetometer option. Approximately

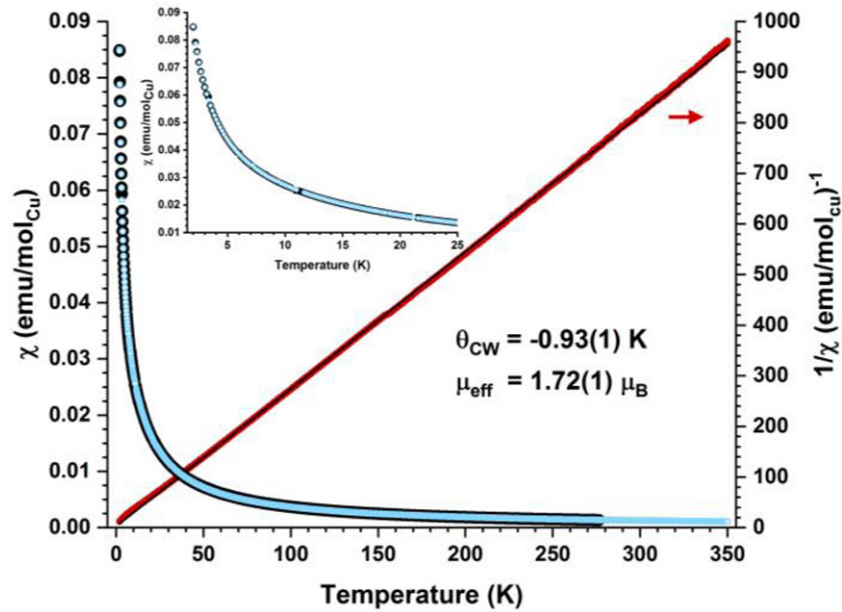


**Figure 4.** Magnetic susceptibility data for the  $\text{Ca}_3\text{Cu}_2\text{GeV}_2\text{O}_{12}$  garnet. The field cooled data are shown with open light-blue circles, while the zero-field cooled data are shown with solid black circles. The closed red circles show the inverse magnetic susceptibility data and the black line is the fit to the Curie–Weiss law. All data were collected in a 0.1 T field. Note:  $1 \text{ emu}/(\text{mol Oe}) = 4\pi \cdot 10^{-6} \text{ m}^3 \text{ mol}^{-1}$ .

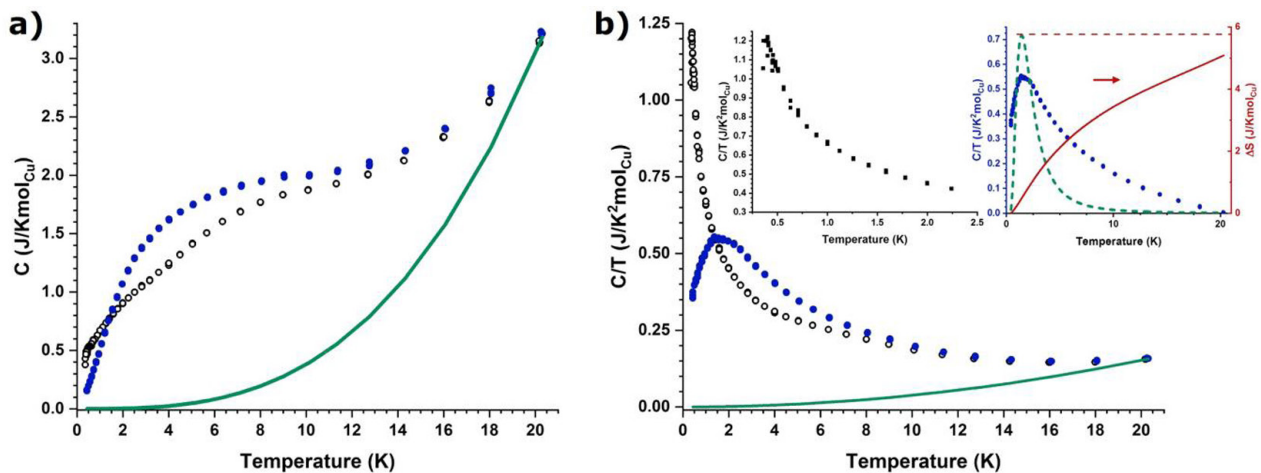


**Figure 5.** Specific heat measurements of:  $\text{Ca}_3\text{Cu}_2\text{GeV}_2\text{O}_{12}$  at 0 T (open black circles), 9 T (solid blue circles); and  $\text{Ca}_3\text{Mg}_2\text{GeV}_2\text{O}_{12}$  (green line) used as a lattice standard. a) Heat capacity as a function of temperature. (b)  $C/T$  as a function of temperature. Inset (left) shows a zoom window of the data at 0 T, while inset (right) shows the lattice subtracted 3 T data for  $\text{Ca}_3\text{Cu}_2\text{GeV}_2\text{O}_{12}$  as solid blue circles with the dashed green line representing the best fit to the Schottky model. The solid red line represents the integration from 350 mK to 20 K and the red dashed line is the expected value for  $R\ln(2S + 1)$  with  $S = \frac{1}{2}$ .

25 mg of sample were measured from 1.8 K to 350 K in a 0.1 T applied magnetic field.

#### 2.4. Heat capacity

Heat capacity measurements were collected on an approximately 6 mg pellet adhered to a sapphire platform sample stage of a Quantum Design Helium-3 insert puck using Apiezon N grease. Data were collected using the quasiadiabatic technique at magnetic fields of 0 T and 3 T from 0.350 K to 20 K. The heat capacity of the puck and grease were subtracted from the total heat capacity.

#### 2.5. Neutron diffraction

Neutron diffraction was conducted on the BT-7 triple axis spectrometer at the National Institute of Standards and Technology Center for Neutron Research in Gaithersburg, Maryland, USA [22]. Ten grams of  $\text{Ca}_3\text{Cu}_2\text{GeV}_2\text{O}_{12}$  polycrystalline powder was packed in a copper sample can and pressurized under 10 atmospheres of helium at 300 K in order to improve thermal contact. Neutrons with a wavelength of  $2.359 \text{ \AA}$  were used with open collimation and a position-sensitive detector. A dilution fridge was used to collect data at 10 K, 800 mK, and 70 mK covering a  $2\theta$  range from  $10^\circ$ – $68^\circ$ .

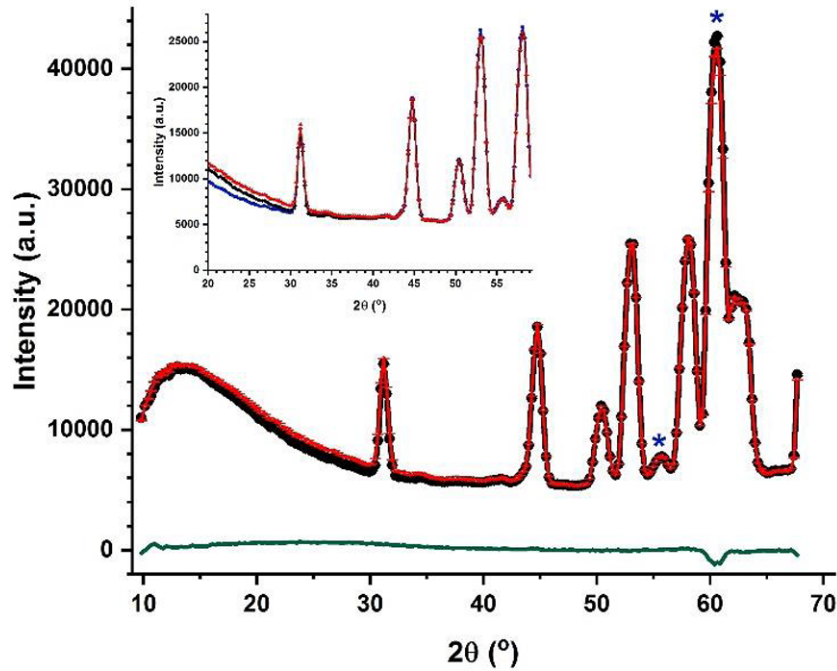


**Figure 6.** Neutron diffraction data for  $\text{Ca}_3\text{Cu}_2\text{GeV}_2\text{O}_{12}$  collected on the BT-7 triple axis spectrometer at the National Institute of Standards and Technology Center for Neutron Research. Diffraction data were collected at 800 mK (black curve) and 70 mK (red curve). The reduction in intensity at the lowest angles is due to attenuation by the Bi shielding in the direct beam. The green curve is the difference between the 800 mK and 70 mK data. Blue asterisks represents peaks from the CuO impurity as well as Al from the cryostat. The inset also includes 10 K data (blue).

### 3. Results and discussion

$\text{Ca}_3\text{Cu}_2\text{GeV}_2\text{O}_{12}$  was synthesized using the conventional solid state method as described in section 2.1. Rietveld refinements against x-ray diffraction data confirm a cubic cell with the space group  $Ia\bar{3}d$  and a lattice parameter of 12.43408(8) Å. The Rietveld refinement is shown in figure 3, and table 1 reports the relevant structural parameters for  $\text{Ca}_3\text{Cu}_2\text{GeV}_2\text{O}_{12}$ . The unidentified peaks present in the work by Mill *et al* [21] are present for all synthesis attempts. They have been identified as a CuO impurity in the range of 1%–5% by weight. In these refinements, the vanadium to germanium ratio was kept at 2:1 and no site mixing was seen for any cations. Diffraction confirms regular dodecahedral, octahedral, and tetrahedral coordination for Ca, Cu, and Ge, respectively, with bond lengths of 2.42856(2) Å for all Ca–O bonds, 2.10272(2) Å for all Cu–O bonds, and 1.74512(1) Å for all Ge–O bonds. Consequently, the Cu–Cu nearest neighbours are 5.38412(4) Å and the second-nearest neighbour Cu–Cu bond is 6.21704(5) Å. These are well within standard bond distances for known copper (II) oxides.

Magnetic susceptibility was collected from 2 K to 350 K (figure 4), showing completely overlapping field cooled and zero-field cooled data. This suggests an absence of glassiness or ferromagnetic phase transitions in the measured temperature range. The inverse susceptibility versus temperature data showed linear behaviour for the full data range. The data were fit to the Curie–Weiss law ( $\chi = C/(T - \theta_{\text{CW}})$ ) where a  $\theta_{\text{CW}}$  of  $-0.93(1)$  K was extracted along with a  $\mu_{\text{eff}}$  of  $1.72(1) \mu_{\text{B}}$ . The effective moment corresponds well with the expected spin-only magnetic moment of  $\text{Cu}^{2+}$  with a spin

of  $S = 1/2$  (using  $\mu = 2[S(S + 1)]^{1/2} = 1.73 \mu_{\text{B}}$ ). The  $\theta_{\text{CW}}$  indicates the presence of net antiferromagnetic interactions in the  $\text{Ca}_3\text{Cu}_2\text{GeV}_2\text{O}_{12}$  ground state. Magnetic susceptibility shows no obvious phase transition to 1.8 K, which is not surprising due to the  $\theta_{\text{CW}} = -0.93(1)$  K. The low value for the Curie–Weiss temperature is surprising, given the extended nature of the d-orbitals for  $\text{Cu}^{2+}$ , and likely is a sign of competing interactions between nearest and next nearest neighbour spins. An estimate of the nearest neighbour  $J_{nn}$  can be made through a mean field approximation [23]:

$$\theta_c = 2S(S + 1) / 3k \sum z_n J_n$$

where  $n$  is the  $n$ th neighbour and  $J_n$  is the corresponding exchange constant,  $S$  is the spin,  $k$  is Boltzmann’s constant,  $z_n$  is the number of neighbours for value  $n$ , and  $\theta_c$  is the algebraic sum of all of the exchange constants [24]. Using this approximation, one can estimate the nearest neighbour exchange constant to be  $J_{nn} = -0.23(1)$  K, and if this system is close to the quantum phase transition,  $J_{nnn} = -0.16(1)$  K.

Heat capacity can be used to explore phase transitions (magnetic or structural) which may exist at low temperature. It is also an important tool used to understand the magnetic entropy at low temperature. As can be seen in figure 5, no magnetic ordering, in the form of a lambda like anomaly for a phase transition, is seen down to 350 mK in zero applied field. There is, however, a sharp increase seen in  $C/T$  (figure 5(b)) at low temperatures. An applied magnetic field pushes this feature out to higher temperatures—the 3 T curves (blue) in figure 5(b) show a peak at 1.4 K in the  $C/T$  versus  $T$  plot for an applied field of 3 T. This is typical of a Schottky anomaly

due to the splitting of the low temperature  $S = 1/2$  doublet in a magnetic field. Fits to the Schottky model largely failed in capturing the data, indicating more complicated magnetic interactions at play. Integrating the area between the 3 T curve and the lattice standard ( $\text{Ca}_3\text{Mg}_2\text{GeV}_2\text{O}_{12}$ ) extracts the majority of the entropy expected for a  $S = 1/2$  system. Using the spin-only formula for the expected entropy ( $\Delta S = R \ln(2S + 1)$ ) a value of  $5.76 \text{ J (K mol}_{\text{Cu}})^{-1}$  is expected. The total integration from 350 mK to 20 K yields a value of  $\Delta S = 5.08 \text{ J (K mol}_{\text{Cu}})^{-1}$ . The missing entropy is likely from an inability to integrate the full heat capacity peak at low temperatures.

Neutron diffraction using a dilution refrigerator (resulting in an aluminum peak around  $2\theta = 60^\circ$ ) was used in order to further probe the possible ordering temperature of  $\text{Ca}_3\text{Cu}_2\text{GeV}_2\text{O}_{12}$  and determine which of the antiferromagnetic structures predicted by Oitmaa and Zheng might be present below the ordering temperature [15]. Figure 6 shows the comparison of diffractograms taken at 800 mK and 70 mK. As can be seen by the difference line the only difference between the two temperatures is found in the peak at  $2\theta = 60^\circ$ , which does not belong to the sample. The inset also includes the data collected at 10 K showing no difference in  $\text{Ca}_3\text{Cu}_2\text{GeV}_2\text{O}_{12}$  peak size or shape, and no new peaks appearing. This suggests that in the absence of field, no long range ordering occurs down to 70 mK. A frustration parameter ( $f = |\theta_{\text{CW}}|/T_c$ ) is often used to indicate how frustrated a system is. Ideally, a quantum spin liquid would show a frustration parameter of infinity, as there is no ordering down to 0 K [25]. Highly frustrated systems typically have  $f > 10$  [24, 26]. A minimum value of  $f = 13.29$  can be calculated based on no magnetic ordering down to 0.07 K, confirming that our system is highly frustrated and a possible spin liquid candidate. The proximity to a possible quantum phase transition for competing  $J_2/J_1$  interactions on the  $S = 1/2$  BCC lattice is a likely origin for this phase.

#### 4. Conclusions

The quantum spin liquid candidate  $\text{Ca}_3\text{Cu}_2\text{GeV}_2\text{O}_{12}$  was explored using x-ray and neutron diffraction, confirming the successful synthesis of the garnet phase (s.g. 230:  $Ia\bar{3}d$ ) with no magnetic phase transitions down to 70 mK. Magnetic susceptibility confirms the  $\text{Cu}^{2+}$  magnetic ion is present and that net antiferromagnetic interactions dominate. Specific heat measurements suggest no long range order down to base temperature of 350 mK and low temperature neutron diffraction suggests this lack of magnetic order extends to temperatures beyond 70 mK. Providing unambiguous evidence of a quantum spin liquid is a difficult task, and many more experiments, such as thermal transport [27] and inelastic neutron scattering measurements [28], are required before any confirmation of this elusive phase can be claimed. However, this work shows that  $\text{Ca}_3\text{Cu}_2\text{GeV}_2\text{O}_{12}$  is a promising material in the search for quantum spin liquids and that using the competing exchange interactions on the B-site of the garnet phase with a spin =  $1/2$  magnetic ion shows promise for future quantum spin liquid research.

#### Acknowledgments

CRW acknowledges support for this work through NSERC (DG and CRC), the CFI, and CIFAR. We acknowledge the support of the National Institute of Standards and Technology, U.S. Department of Commerce, in providing the neutron research facilities used in this work. The identification of any commercial product or trade name does not imply endorsement or recommendation by the National Institute of Standards and Technology.

#### ORCID iDs

Joey A Lussier  <https://orcid.org/0000-0003-3589-6938>

Cole Mauws  <https://orcid.org/0000-0003-1826-6432>

Chris R Wiebe  <https://orcid.org/0000-0002-3681-0182>

#### References

- [1] Zhou Y, Kanoda K and Ng T K 2017 Quantum spin liquid states *Rev. Mod. Phys.* **89** 025003
- [2] Gingras M J P and McClarty P A 2014 Quantum spin ice: a search for gapless quantum spin liquids in pyrochlore magnets *Rep. Prog. Phys.* **77** 056501
- [3] Chalker J T 2011 Geometrically frustrated antiferromagnets: statistical mechanics and dynamics *Introduction to Frustrated Magnetism* ed C Lacroix et al (Berlin: Springer) pp 3–22
- [4] Chandra P and Doucot B 1988 Possible spin-liquid state at large S for the frustrated square Heisenberg lattice *Phys. Rev. B* **38** 9335–8
- [5] Sushkov O P, Oitmaa J and Weihong Z 2001 Quantum phase transition in the two-dimensional  $J_1$ – $J_2$  model *Phys. Rev. B* **63** 104420
- [6] Savary L and Balents L 2017 Quantum spin liquids: a review *Reports Prog. Phys.* **80**
- [7] Knolle J and Moessner R 2019 A field guide to spin liquids *Annu. Rev. Condens. Matter Phys.* **10** 451–72
- [8] Misguich G 2011 Quantum spin liquids and fractionalization *Introduction to Frustrated Magnetism* ed C Lacroix et al (Berlin: Springer) pp 407–35
- [9] Balents L 2010 Spin liquids in frustrated magnets *Nature* **464** 199–208
- [10] Wen J, Yu S L, Li S, Yu W and Li J X 2019 Experimental identification of quantum spin liquids *NPJ Quantum Mater.* **4** 12
- [11] Han T H, Helton J S, Chu S Y, Nocera D G, Rodriguez-Rivera J A, Broholm C and Lee Y S 2012 Fractionalized excitations in the spin-liquid state of a kagome-lattice antiferromagnet *Nature* **492** 406–10
- [12] Clark L et al 2019 Two-dimensional spin liquid behaviour in the triangular-honeycomb antiferromagnet  $\text{TbInO}_3$  *Nat. Phys.* **15** 262–8
- [13] Gardner J S, Gingras M J P and Greedan J E 2010 *Rev. Mod. Phys.* **82** 53
- [14] Wiebe C R, Greedan J E, Luke G M and Gardner J S 2002 *Phys. Rev. B* **65** 144413
- [15] Oitmaa J and Zheng W 2004 Phase diagram of the bcc  $S = 1/2$  Heisenberg antiferromagnet with first and second neighbor exchange *Phys. Rev. B* **69** 064416
- [16] Ghosh P, Müller T, Toldin F P, Richter J, Narayanan R, Thomale R, Reuther J and Iqbal Y 2019 Quantum paramagnetism and helimagnetic orders in the Heisenberg

- model on the body centered cubic lattice *Phys. Rev. B* **100** 014420
- [17] Grew E S, Locock A J, Mills S J, Galuskina I O, Galuskin E V and Halenius U 2013 Nomenclature of the garnet supergroup *Am. Mineral.* **98** 785–811
- [18] Bayer G 1965 Vanadates  $A_3B_2V_3O_{12}$  with garnet structure *J. Am. Ceram. Soc.* **48** 600
- [19] Hrichova R 1970 Synthesis of Mn vanadates with the garnet structure *J. Am. Ceram. Soc.* **53** 112
- [20] Neurgaonkar R R and Hummel F A 1975 Substitutions in vanadate garnets *Mater. Res. Bull.* **10** 51–6
- [21] Mill B V, Ronniger G and Kabalov Y K 2014 New garnet compounds ( $A = Ca, Cd$ ;  $B = Mg, Zn, Co, Ni, Cu, Mn, Cd$ ;  $C = Ge, Si$ ) *Russ. J. Inorg. Chem.* **59** 1208–13
- [22] Lynn J W, Chen Y, Chang S, Zhao Y, Chi S, Ratcliff W, Ueland B G, Erwin R W and Erwin R W 2012 Double-focusing thermal triple-axis spectrometer at the NCNR *J. Res. Natl Inst. Stand. Technol.* **117** 61–79
- [23] Smart J S 1966 *Effective Field Theories of Magnetism* (Philadelphia, PA: W. B. Sanders)
- [24] Greedan J E 2001 Geometrically frustrated magnetic materials *J. Mater. Chem.* **11** 37–53
- [25] Norman M R 2016 Colloquium: Herbertsmithite and the search for the quantum spin liquid *Rev. Mod. Phys.* **88** 041002
- [26] Ramirez A P 1994 Strongly geometrically frustrated magnets *Annu. Rev. Mater. Sci.* **24** 453–80
- [27] Katsura H, Nagaosa N and Lee P A 2010 Theory of the thermal Hall effect in quantum magnets *Phys. Rev. Lett.* **104** 066403
- [28] Helton J S *et al* 2007 Spin dynamics of the spin-1/2 Kagome lattice antiferromagnet  $ZnCu_3(OH)_6Cl$  *Phys. Rev. Lett.* **98** 107204